JACS
JOURNAL OF THE AMERICAN CHEMICAL SOCIETY
Article
pubs.acs.org/JACS

Laser-Induced Dynamics of Peroxodicopper(II) Complexes Vary with the Ligand Architecture. One-Photon Two-Electron O_2 Ejection and Formation of Mixed-Valent Cu^ICu^{II}–Superoxide Intermediates

Claudio Saracini,[†] Kei Ohkubo,[‡,§] Tomoyoshi Suenobu,[‡] Gerald J. Meyer,[†,⊥] Kenneth D. Karlin,*[,†] and Shunichi Fukuzumi*[,‡,§,∥]

[†]Department of Chemistry, The Johns Hopkins University, Baltimore, Maryland 21218, United States
[‡]Department of Material and Life Science, Graduate School of Engineering, Osaka University, ALCA and SENTAN, Japan Science and Technology Agency (JST), Suita, Osaka 565-0871, Japan
[§]Department of Chemistry and Nano Science, Ewha Womans University, Seoul 120-750, Korea
[∥]Faculty of Science and Engineering, Meijo University, ALCA and SENTAN, Japan Science and Technology Agency (JST), Nagoya, Aichi 468-0073, Japan

Supporting Information

ABSTRACT: Photoexcitation of end-on *trans*-μ-1,2-peroxodicopper(II) complex $[(tmpa)_2Cu^{II}_2(O_2)]^{2+}$ (**1**) (λ_{max} = 525 and 600 nm) and side-on μ-η^2:η^2-peroxodicopper(II) complexes $[(N5)Cu^{II}_2(O_2)]^{2+}$ (**2**) and $[(N3)Cu^{II}_2(O_2)]^{2+}$ (**3**) at −80 °C in acetone led to one-photon two-electron peroxide-to-dioxygen oxidation chemistry ($O_2^{2-} + h\nu \rightarrow O_2 + 2e^-$). Interestingly, light excitation of **2** and **3** (having side-on μ-η^2:η^2-peroxo ligation) led to release of dioxygen, while photoexcitation of **1** (having an end-on *trans*-1,2-peroxo geometry) did not, even though spectroscopic studies revealed that both reactions proceeded through previously unknown mixed-valent superoxide species: $[Cu^{II}(O_2^{\bullet-})Cu^I]^{2+}$ (λ_{max} = 685−740 nm). For **1**, this intermediate underwent further fast intramolecular electron transfer to yield an "O_2-caged" dicopper(I) adduct, Cu^I_2–O_2, and a barrierless stepwise back electron transfer to regenerate **1** occurred. Femtosecond laser excitation of **2** and **3** under the same conditions still led to $[Cu^{II}(O_2^{\bullet-})Cu^I]^{2+}$ intermediates that, instead, underwent O_2 release with a quantum yield of 0.14 ± 0.1 for **3**. Such remarkable differences in reaction pathways likely result from the well-known ligand-derived stability of **2** and **3** vs **1** indicated by ligand–$Cu^{II/I}$ redox potentials; (N5)Cu^I and (N3)Cu^I complexes are far more stable than (tmpa)Cu^I species. The fast Cu^I_2/O_2 rebinding kinetics was also measured after photoexcitation of **2** and **3**, with the results closely tracking those known for the dicopper proteins hemocyanin and tyrosinase, for which the synthetic dicopper(I) precursors $[(N5)Cu^I_2]^{2+}$ and $[(N3)Cu^I_2]^{2+}$ and their dioxygen adducts serve as models. The biological relevance of the present findings is discussed, including the potential impact on the solar water splitting process.

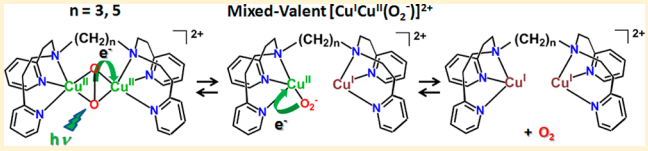

INTRODUCTION

Copper–dioxygen intermediates play key roles in chemically mediated oxidation reactions, and in copper proteins involved in dioxygen (O_2) processing for reversible O_2 binding, O_2 activation leading to substrate oxidations (e.g., in monooxygenases), or protein oxidase reduction of O_2 to produce H_2O_2 or water. Among copper–dioxygen adducts, several types of peroxodicopper(II) complexes have been well-characterized, with the type of coordination/structure dictated by the nature (denticity, donor atom type, etc.) of the ligand bound to the copper ion. Prominent among these are the end-on *trans*-μ-1,2-peroxodicopper(II) (^{T}**P**) and μ-η^2:η^2-peroxodicopper (^{S}**P**) species; either of these may isomerize to the bis(μ-oxo)-dicopper(III) complexes (**O**) (Scheme 1).[1−10] All of these Cu^I/O_2-derived dicopper product species have been studied extensively with respect to their inherent or comparative spectroscopic signatures; their differential reactivity with substrates has also been widely investigated.[11−19]

Scheme 1

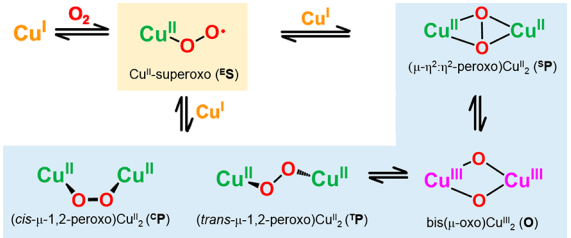

Furthermore, these Cu_2–O_2 species are strong light absorbers, with prominent UV and/or visible region peroxo- or oxo-to-copper ion charge transfer transitions. In fact, there are now a few cases known where laser-induced photolysis excitation leads to photoejection of molecular oxygen, two

Received: September 28, 2015
Published: December 11, 2015

DOI: 10.1021/jacs.5b10177
J. Am. Chem. Soc. 2015, 137, 15865−15874

being synthetic cupric superoxide (^{E}**S**) coordination complexes,[18a] with the others including protein $Cu_2(O_2)$ adducts.[20] For such cases, nanosecond laser flash photolysis can be used to follow the rebinding kinetics–thermodynamics of O_2 to the copper(I) species produced for systems that bind molecular oxygen faster than can be followed by solution spectroscopic stopped-flow kinetic methods.[14a,b,d–g]

On the other hand, the identification, characterization, or investigation of the dynamics of photoexcited states has been an elusive subject since (i) they are very short-lived and (ii) these solution-phase Cu–dioxygen adducts (i.e., **1**, **2**, **3**, or similar) are generally only stable at low temperatures (<−80 °C), precluding the investigation of excited-state fast photodynamics using femtosecond laser flash photolysis, normally measured at room temperature.

In the present work, we adjusted the instrumental conditions (see the Experimental Section) to enable low-temperature (−55 to −94 °C) solution femtosecond laser-induced excited-state dynamics studies. When the new apparatus is used to study well-known peroxodicopper(II) complexes, it becomes possible to detect and characterize unprecedented and perhaps unexpected (vide infra) mixed-valent transient $Cu^{I}Cu^{II}$–superoxide species. Furthermore, monitoring of their subsequent fast (i.e., picosecond) reaction dynamics has also become achievable. The species studied and described here are the ^{T}**P** complex $[(tmpa)Cu^{II}(O_2)Cu^{II}(tmpa)]^{2+}$ (**1**) {tmpa = tris(2-pyridylmethyl)amine}[7] and the complexes with side-on O_2^{2-} binding, μ-η^2:η^2-peroxodicopper(II) complexes $[(N5)Cu^{II}_2(O_2)]^{2+}$ (**2**) {N5 = $(CH_2)_5$-linked bis[(2-(2-pyridyl)ethyl)amine]) (PY2) units} and $[(N3)Cu^{II}_2(O_2)]^{2+}$ (**3**) {N3 = $(CH_2)_3$-linked PY2 units} (Chart 1).[8c–e]

Chart 1

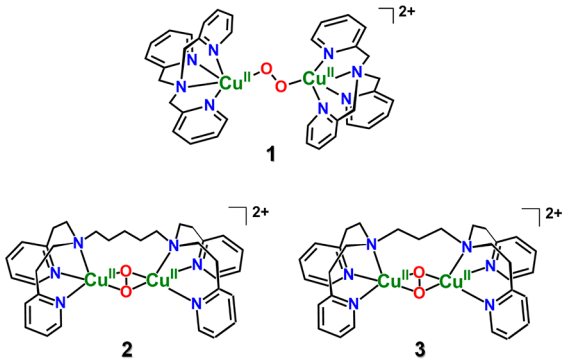

Interestingly, the nature of the excited-state species formed was similar in all cases (**1**–**3**): a previously unobserved Cu^{II}–superoxide···Cu^{I} species, ($[Cu^{II}(O_2^{\bullet-})Cu^{I}]^{2+}$). Subsequent novel transformations occurred, and UV–vis spectroscopic monitoring allowed for the determination of the kinetic and activation parameters. Notably, the two varying classes of compounds, represented by end-on (**1**) and side-on (**2** and **3**) peroxodicopper(II) complexes, follow unique reaction pathways. The differential behavior can be explained on the basis of the nature of the ligands employed within these complexes (Chart 1), which influenced the thermodynamic stabilities of (i) the ligand–Cu^{I} (vs Cu^{II}) complexes and (ii) peroxo–Cu_2^{II} structures. The present study opens an exciting research area on reactive excited states of metal–O_2 intermediates.

RESULTS AND DISCUSSION

Photodynamics of Peroxo (^{T}P) Complex $[(tmpa)Cu^{II}(O_2)Cu^{II}(tmpa)]^{2+}$ (1). The previously well-characterized end-on *trans*-μ-1,2-peroxo dinuclear copper(II) complex **1** was prepared by reaction of $[(tmpa)Cu^{I}(CH_3CN)]BArF$ (BArF = $B(C_6F_5)_4^-$) with O_2 at low temperature in acetone (Figure 1a,

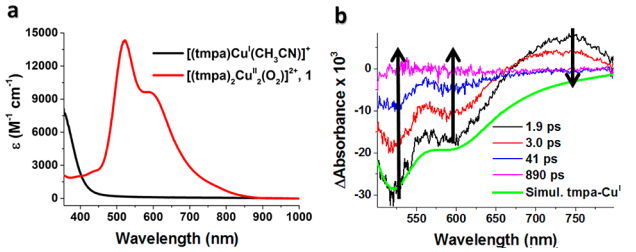

Figure 1. (a) Absorption spectrum of **1** (red line) obtained from oxygenation of $[(tmpa)Cu^{I}(CH_3CN)]^{+}$ (black line) at −80 °C in acetone. (b) Transient difference absorption spectra of **1** in acetone at −80 °C measured at the indicated delay times after 490 nm femtosecond laser excitation (2 mJ/pulse and fwhm = 130 fs). Overlaid in green is a simulated spectrum for **1**, generated by subtraction of the red spectrum from the black spectrum shown in (a).

red spectrum) at −80 °C.[7] The complex was brightly colored due to the presence of intense peroxo-to-copper charge transfer bands in the visible region. The transient absorption spectrum measured 1.9 ps after femtosecond laser excitation of **1** exhibited a positive absorption band at λ_{max} = 739 nm and negative absorption difference (bleaching) features at λ_{max} = 525 and 600 nm, Figure 1b. The bleach features were a mirror image of the steady-state absorption spectrum of **1**, consistent with the loss of the ground-state species. Indeed, a simulation based on the assumption that light excitation of **1** generated a species that did not absorb visible light accurately models the two bleach absorption bands at λ_{max} = 525 and 600 nm. However, such modeling did not explain the positive absorption band at λ_{max} = 739 nm. The observed absorption maximum and full width at half-maximum were similar to those previously reported for Cu^{II}–superoxide complexes $[(tmpa)Cu^{II}(O_2)]^{+}$,[14b] $[(TMG_3tren)Cu^{II}(O_2)]^{+}$,[18] $[(PV\text{-}tmpa)Cu^{II}(O_2)]^{+}$ (PV-tmpa = [bis(pyrid-2-ylmethyl)[(6-pivalamidopyrid-2-yl)methyl]amine]),[19] as well as to those of several other known copper(II)–superoxide compounds.[21,22] On the basis of these prior data, the transient absorption spectrum observed upon femtosecond laser excitation of **1** (black line in Figure 1b) was assigned to the mixed-valent Cu^{I}–Cu^{II}–superoxide ($O_2^{\bullet-}$) complex $[(tmpa)Cu^{II}(O_2^{\bullet-})Cu^{I}(tmpa)]^{2+}$ produced by intramolecular electron transfer from the peroxo moiety to one of the two Cu^{II} centers in the Franck–Condon excited state **1***(Scheme 2).

Very similar absorption features were observed after pulsed laser excitation of **2** and **3** under the same conditions. The absorption maxima for the positive absorption feature assigned to the mixed-valent intermediates were determined from Gaussian fits of the observed data (Figure S1). A linear relationship between the absorption change at 750 nm,[23] due to the Cu^{I}–Cu^{II}–superoxide ($O_2^{\bullet-}$) complex $[(tmpa)Cu^{II}(O_2^{\bullet-})Cu^{I}(tmpa)]^{2+}$, and the laser fluence was observed over a range of 11–46 μJ/pulse, consistent with a monophotonic process in the formation of the Cu^{II}–$O_2^{\bullet-}$–Cu^{I} complex (Figure S2a in the Supporting Information).

DOI: 10.1021/jacs.5b10177
J. Am. Chem. Soc. 2015, 137, 15865–15874

Scheme 2

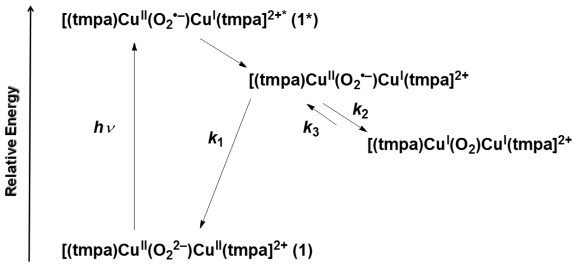

To confirm that the chemistry described here (vide supra) was truly due to the light-induced reaction of the peroxo complex $[(tmpa)Cu^{II}(O_2)Cu^{II}(tmpa)]^{2+}$ (**1**), control experiments were carried out. No photoactivity was observed after irradiation of either the mononuclear tmpa−copper(I) precursor complex alone or the decomposition products of **1** (formed by warming a cryogenically produced solution of **1** to room temperature) and subsequent rechilling.

Further Reactions of $[(tmpa)Cu^{II}(O_2^{\bullet-})Cu^{I}(tmpa)]^{2+}$ (λ_{max}, 739 nm). Single-wavelength kinetics monitored at 600 and 750 nm are shown in Figure 2. The fastest decay, observed

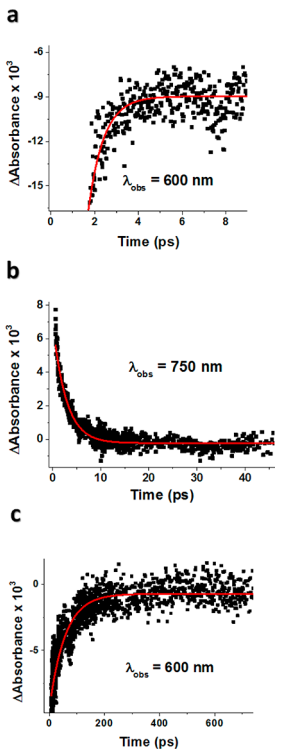

Figure 2. Time courses of femtosecond laser-induced reactions of **1** in acetone at −80 °C. Overlaid in red are fits to first-order kinetic models. (a) Fast partial recovery of the bleaching at 600 nm. (b) Decay of the absorbance difference observed at 750 nm due to the complex $([(tmpa)Cu^{II}(O_2^{\bullet-})Cu^{I}(tmpa)]^{2+})$. (c) Slower recovery of the bleaching observed at 600 nm to completely regenerate **1**.

within the first 5 ps after laser excitation of **1**, was the partial recovery of the bleach at 600 nm that occurs with a first-order rate constant $k_1 = (2.8 \pm 0.4) \times 10^{12}$ s^{-1} (Figure 2a). This corresponds to back electron transfer from the Cu^{I} center to $O_2^{\bullet-}$ to regenerate **1** from the mixed-valent $Cu^{II}-O_2^{\bullet-}-Cu^{I}$ intermediate (k_1 in Scheme 2): $Cu^{II}-O_2^{\bullet-}-Cu^{I} \rightarrow Cu^{II}-O_2^{2-}-Cu^{II}$ (**1**). In fact, the same rate constant ($(2.3 \pm 0.3) \times 10^{12}$ s^{-1}, Figure S2b in the Supporting Information) was abstracted from the early data collected at 750 nm. The amplitude change measured at 750 nm revealed that ∼90% of the mixed-valent species converted to the ground state **1** within the first few picoseconds. A more precise value was precluded as overlap with a second kinetic process disallowed our ability to accurately quantify the amplitude (k_2; vide infra).

On the other hand, the absorption decay at 750 nm occurring with a rate constant $k_2 = (4.0 \pm 0.5) \times 10^{11}$ s^{-1} at −80 °C, due to the disappearance of the $Cu^{II}-O_2^{\bullet-}$ moiety in the mixed-valent intermediate (Figure 2b), is significantly slower than the fast partial bleach recovery observed at 600 nm. This indicates that a second process involving electron transfer was operative, that from the $O_2^{\bullet-}$ moiety to the Cu^{II} center, to produce what formally is to be considered as a $Cu^{I}_2-O_2$ complex $([(tmpa)Cu^{I}(O_2)Cu^{I}(tmpa)]^{2+}$, a "caged" O_2 species. Assuming that this caged species does not absorb light at 750 nm, about 10% of the mixed-valent complexes reacted to form this caged O_2 species, $Cu^{II}-O_2^{\bullet-}-Cu^{I} \rightarrow Cu^{I}-O_2-Cu^{I}$, k_2 in Scheme 2.

The slow bleach recovery monitored at 600 nm corresponds to the stepwise back electron transfer from the two Cu^{I} centers to the O_2 moiety in the $Cu^{I}_2-O_2$ complex to regenerate **1** with a rate constant $k_3 = (1.8 \pm 0.1) \times 10^{10}$ s^{-1} (Figure 2c). In this case, the rate-determining step is an uphill back electron transfer from one Cu^{I} center to the O_2 moiety in the $Cu^{I}_2-O_2$ complex $(Cu^{I}-O_2-Cu^{I} \rightarrow Cu^{II}-O_2^{\bullet-}-Cu^{I})$ followed by the much faster ($k_1 \gg k_3$; vide supra) second step back electron transfer from the other Cu^{I} center to the superoxide moiety in the $Cu^{II}-O_2^{\bullet-}-Cu^{I}$ complex to give back **1** $(Cu^{II}-O_2^{\bullet-}-Cu^{I} \rightarrow Cu^{II}-O_2^{2-}-Cu^{II})$.

The temperature dependence of the rate constants k_1, k_2, and k_3 was examined in the temperature range from −94 to −55 °C, and the rate constants determined are listed in Tables S1, S2, and S3, respectively, of the Supporting Information. An Eyring plot of k_1 for the electron transfer from the Cu^{I} center to the $O_2^{\bullet-}$ moiety in the mixed-valent $Cu^{II}-O_2^{\bullet-}-Cu^{I}$ complex $([(tmpa)Cu^{II}(O_2^{\bullet-})Cu^{I}(tmpa)]^{2+})$ to regenerate **1** is shown in Figure 3, where k_1 is seen to be nearly temperature independent.

The $\Delta H^{\ddagger}$ and $\Delta S^{\ddagger}$ values obtained are listed in Table 1. For k_1, both values were virtually zero. Such a small activation entropy is typical for an electron transfer process involving no bond breaking. Thus, electron transfer from the Cu^{I} center to

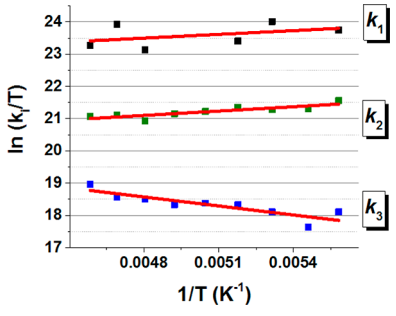

Figure 3. Eyring plots of k_1 (electron transfer from the Cu^{I} center to the $O_2^{\bullet-}$ moiety in the $Cu^{II}-O_2^{\bullet-}-Cu^{I}$ complex to regenerate **1**), k_2 (electron transfer from the $O_2^{\bullet-}$ moiety to the Cu^{II} center in $[(tmpa)Cu^{II}(O_2^{\bullet-})Cu^{I}(tmpa)]^{2+}$ to produce the "in-cage" $Cu^{I}_2-O_2$ complex), and k_3 (stepwise back electron transfer reaction from the Cu^{I} centers to the O_2 moiety in the $Cu^{I}_2-O_2$ intermediate to regenerate the peroxo complex $[(tmpa)Cu^{II}(O_2)Cu^{II}(tmpa)]^{2+}$ (**1**)).

DOI: 10.1021/jacs.5b10177
J. Am. Chem. Soc. 2015, 137, 15865−15874

Table 1. Kinetic Parameters for Femtosecond Laser-Induced Reactions of 1 at −80 °C

	rate constant, s^{-1}	$\Delta H^{\ddagger}$ [a]	$\Delta S^{\ddagger}$ [b]	$\Delta G^{\ddagger}$ [a]
k_1	$(2.8 \pm 0.4) \times 10^{12}$	-0.8 ± 0.8	-4 ± 4	0.0 ± 0.8
k_2	$(4.0 \pm 0.1) \times 10^{11}$	-0.5 ± 0.4	-7 ± 5	0.9 ± 0.4
k_3	$(1.8 \pm 0.1) \times 10^{10}$	1.9 ± 0.4	-4 ± 5	2.7 ± 0.4

[a]Units for $\Delta H^{\ddagger}$ and $\Delta G^{\ddagger}$(−80 °C) are kcal mol^{-1} [b]Units for $\Delta S^{\ddagger}$ are cal K^{-1} mol^{-1}.

the $O_2^{\bullet-}$ moiety in the $Cu^{II}-O_2^{\bullet-}-Cu^{I}$ complex is a barrierless adiabatic process. Because the activation entropy for k_1 is nearly zero (Table 1), it is likely that a cupric superoxide $Cu^{II}-O-O^{\bullet-}$ end-on structure is maintained in the $Cu^{II}-O_2^{\bullet-}-Cu^{I}$ complex, similar to that found in the μ-1,2-peroxo complex **1** (see Chart 1 and Scheme 3).

Scheme 3

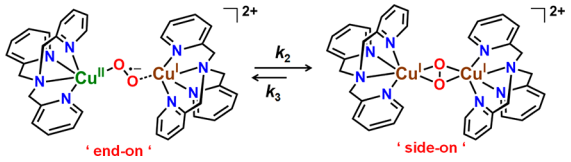

The Eyring plot related to k_2 for the electron transfer from the $O_2^{\bullet-}$ moiety to the Cu^{II} center to produce the $Cu^{I}{}_2-O_2$ complex is also shown in Figure 3, where k_2 was nearly temperature independent, as was the case for k_1. Because no O_2 release was observed from this $Cu^{I}{}_2-O_2$ complex, we postulate that O_2 remains in a complex cage; furthermore, the observed negative activation entropy suggests that the geometry of O_2 in the $Cu^{I}{}_2-O_2$ complex is more restricted in the transition state; this could indicate, we speculate, that the binding mode of dioxygen changed to a side-on configuration also in the "in-cage" $Cu^{I}(O_2)Cu^{I}$ complex, in contrast with that of the end-on geometry of **1** (Scheme 3).

The Eyring plot of the rate constant k_3 for the back electron transfer from the Cu^{I} center to the O_2 in the $Cu^{I}{}_2-O_2$ complex (Figure 3) afforded a positive activation enthalpy ($\Delta H^{\ddagger}$ = 1.9 ± 0.4 kcal mol^{-1}) and a nearly zero activation entropy ($\Delta S^{\ddagger}$ = −4 ± 5 cal K^{-1} mol^{-1}). The positive activation enthalpy is consistent with the barrierless electron transfer found for the reverse process (k_2 in Scheme 2); because of that, the back electron transfer from one of the two Cu^{I} centers to the O_2 moiety (k_3) must be uphill, as shown in Scheme 2. The subsequent electron transfer from the other Cu^{I} center to the $O_2^{\bullet-}$ moiety to regenerate **1** (k_1) is barrierless (vide supra) and much faster than the rate-determining back electron transfer from the Cu^{I} center to the O_2 moiety ($k_1 \gg k_3$). The $\Delta H^{\ddagger}$ value found here for k_3 (1.9 ± 0.4 kcal mol^{-1}) is similar to that previously determined for the *intermolecular* electron transfer from $[(tmpa)Cu^{I}]^{+}$ to O_2 to produce the superoxide complex $[(tmpa)Cu^{II}O_2]^{+}$ ($\Delta H^{\ddagger}$ = 1.8 kcal mol^{-1}).[14b] In the case of this *intermolecular* electron transfer reaction, however, the $\Delta S^{\ddagger}$ value (−10 cal K^{-1} mol^{-1})[14b] was much more negative than that of the *intramolecular* electron transfer reaction shown in Scheme 2 (virtually zero; vide supra). This is consistent with the fact that an *intermolecular* electron transfer should involve a negative activation entropy because it requires diffusion and the formation of a precursor complex prior to electron transfer, a requirement, instead, not necessary for the *intramolecular* electron transfer process observed here.

The lack of O_2 release from the $Cu^{I}{}_2-O_2$ complex may be attributed to the high activation free energy barrier that needs to be overcome ($\Delta G^{\ddagger} \approx 20$ kcal mol^{-1} at −80 °C) to produce 2 equiv of $[(tmpa)Cu^{I}]^{+}$ and O_2, which are ∼5 kcal mol^{-1} uphill as compared to the $Cu^{I}{}_2-O_2$ adduct, according to data previously reported for this reaction in THF solvent.[7,14a,b]

Photodynamics of Side-On Peroxo Dinuclear Copper(II) Complexes. The results on the end-on peroxo complex **1** described above are in sharp contrast to those observed for the side-on peroxo compound **2** ($[(N5)Cu^{II}(O_2^{2-})Cu^{II}]^{2+}$),[8c−e] where O_2 was instead released after laser excitation of the complex. The adduct **2** was produced by the reaction of $[(N5)Cu^{I}{}_2(CH_3CN)]^{2+}$ with O_2 in acetone at −80 °C, and its electronic spectrum exhibits absorption bands at 360 nm (21 800 M^{-1} cm^{-1}) and at 430 nm (5200 M^{-1} cm^{-1}), which have been previously assigned as peroxide-to-copper(II) ligand-to-metal charge transfer (LMCT) transitions.[8c−e]

Femtosecond laser excitation of **2** in acetone at −94 °C resulted in observation of a transient absorption feature at λ_{max} = 709 nm (Figure 4) which was consistent with the commonly

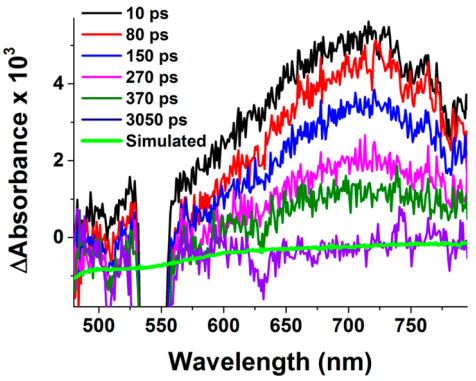

Figure 4. Transient absorption difference spectra of **2** in acetone at −94 °C measured at the indicated delay times after 436 nm femtosecond laser excitation (2 mJ/pulse and fwhm = 130 fs). Overlaid in green is a simulated spectrum for the conversion of peroxo complex **2** to its dicopper(I) precursor plus dioxygen, based on subtraction of the red spectrum from the black spectrum, those shown in Figure 7a. The probe light is interrupted by the pump laser in the wavelength region around 540 nm.

observed low-energy but strong absorption peaks known for Cu^{II}−superoxide complexes.[14b,18,19,21,22] Thus, the transient absorption spectrum observed upon femtosecond laser excitation of **2** in Figure 4 can also be assigned to a mixed-valent $Cu^{II}-O_2^{\bullet-}-Cu^{I}$ complex ($[(N5)Cu^{II}(O_2^{\bullet-})Cu^{I}]^{2+}$) produced by intramolecular electron transfer from the peroxo ligand to the Cu^{II} center via the Franck−Condon LMCT excited state **2*** shown in Scheme 4.

The decay of the absorption due to the $Cu^{II}-O_2^{\bullet-}-Cu^{I}$ complex derived from **2** in acetone at −80 °C, monitored at 720 nm, obeyed first-order kinetics with a rate constant (k_4 in Scheme 4) of $(3.9 \pm 0.3) \times 10^9$ s^{-1}, which is much smaller than that derived for **1** [$(4.0 \pm 0.1) \times 10^{11}$ s^{-1}]. Representative kinetic data collected at −94 °C are shown in Figure 5.

The temperature dependence of the rate constant k_4 was also examined in the temperature range from −94 to −55 °C, and the related Eyring plot is shown as an inset in Figure 5, giving $\Delta H^{\ddagger}$ = 5.4 ± 1.0 kcal mol^{-1} and $\Delta S^{\ddagger}$ = −9 ± 5 cal K^{-1} mol^{-1}. The $Cu^{II}-O_2^{\bullet-}-Cu^{I}$ adduct formed from **2** decays much slower than that derived from **1** (smaller decay constant: k_4 <

DOI: 10.1021/jacs.5b10177
J. Am. Chem. Soc. 2015, 137, 15865−15874

Scheme 4

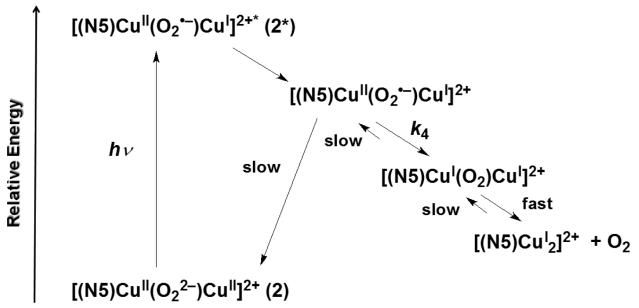

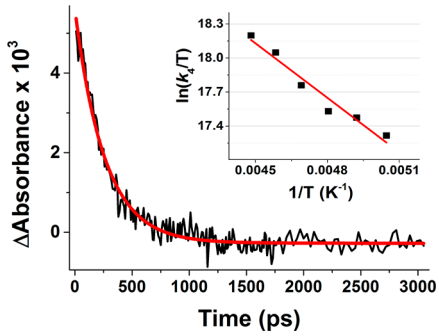

Figure 5. Decay time profile of the absorbance difference observed at 720 nm due to the $Cu^{II}-O_2^{\bullet-}-Cu^{I}$ complex derived from photoexcitation of **2** in acetone at −94 °C. Inset: Eyring plot of k_4 for the intramolecular electron transfer from the $O_2^{\bullet-}$ ligand to the Cu^{II} center in the $Cu^{II}-O_2^{\bullet-}-Cu^{I}$ photoproduct complex derived from **2** in acetone.

k_2) and shows a significantly larger $\Delta H^{\ddagger}$ value. These results are consistent with a larger bond and solvent reorganization energy for the electron transfer from the superoxide anion to Cu^{II} in the $Cu^{II}-O_2^{\bullet-}-Cu^{I}$ photoproduct obtained from laser excitation of $[(N5)Cu^{II}(O_2^{2-})Cu^{II}]^{2+}$ (**2**) with its side-on μ-η^2:η^2-peroxo binding compared to that of the decay of the $Cu^{II}-O_2^{\bullet-}-Cu^{I}$ photoproduct obtained from laser excitation of $[(tmpa)Cu^{II}(O_2^{2-})Cu^{II}(tmpa)]^{2+}$ (**1**) (Scheme 1) with its end-on μ-1,2-peroxo bridging mode.

Femtosecond laser excitation of an acetone solution of the analogue complex $[(N3)Cu^{II}(O_2^{2-})Cu^{II}]^{2+}$ (**3**), supported by a binucleating chelating ligand having a shorter polymethylene chain as compared to **2** (N3 vs N5), also resulted in the formation of a mixed-valent $Cu^{II}-O_2^{\bullet-}-Cu^{I}$ complex: $[(N3)Cu^{II}(O_2^{\bullet-})Cu^{I}]^{2+}$. The latter exhibits a transient absorption signature at λ_{max} = 685 nm (Figure 6).

The observed blue shift of the absorption band of $[(N3)Cu^{II}(O_2^{\bullet-})Cu^{I}]^{2+}$ as compared to that of $[(N5)Cu^{II}(O_2^{\bullet-})Cu^{I}]^{2+}$ (685 nm, Figure 6, vs 709 nm, Figure 4) may be caused by a stronger electrostatic interaction between the Cu^{I} ion and the $O_2^{\bullet-}$ ligand in $[(N3)Cu^{II}(O_2^{\bullet-})Cu^{I}]^{2+}$. This situation could arise because of the Cu^{I} ion's closer spatial proximity as compared to what would be expected in $[(N5)Cu^{II}(O_2^{\bullet-})\cdots Cu^{I}]^{2+}$, due to the difference in the polymethylene chain length in the N3 vs N5 binucleating ligand (see Chart 1). Such differences do manifest themselves in other situations, such as for oxygenation reaction rates of dicopper(I) complexes with N3 vs N5 ligands.[8c,d]

The decay of the absorbance observed at 685 nm obeyed first-order kinetics with a rate constant (k_4) of (7.3 ± 0.3) ×

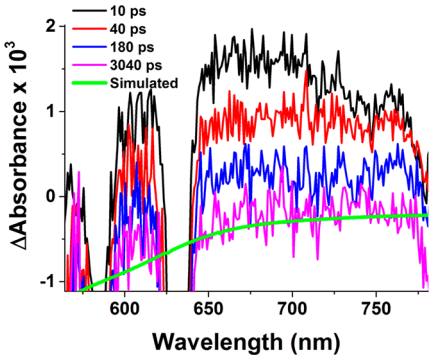

Figure 6. Transient absorption difference spectra of **3** in acetone at −94 °C measured at the indicated delay times after 436 nm femtosecond laser excitation (2 mJ/pulse and fwhm = 130 fs). Overlaid in green is a simulated spectrum for the conversion **3** → Cu^{I} + Cu^{I} + O_2 based on subtraction of the red spectrum from the black shown in Figure 8a. The probe light is interrupted by the pump laser in the wavelength region around 580 and 630 nm.

10^9 s^{-1} (Figure S3 of the Supporting Information), which was larger than that derived from **2** [(3.9 ± 0.1) × 10^9 s^{-1}].

The energy diagram for the femtosecond laser-induced reactions of **2** is shown in Scheme 4. Femtosecond laser excitation into the lower energy LMCT band of **2** resulted in formation of the mixed-valent $Cu^{II}-O_2^{\bullet-}-Cu^{I}$ complex ($[(N5)Cu^{II}(O_2^{\bullet-})Cu^{I}]^{2+}$), which decays via intramolecular electron transfer from the $O_2^{\bullet-}$ ligand to the Cu^{II} center to produce $[(N5)Cu^{I}_2]^{2+}$ with release of molecular oxygen. The finding of O_2 release from the $Cu^{I}_2-O_2$ complex (Scheme 4) is in sharp contrast to the case of **1** (Scheme 2), where back electron transfer from the Cu^{I} center to the O_2 moiety to regenerate **1** occurs without release of O_2. The same energy diagram drawn for **2** can be applied to **3**.

Photodynamics of Side-On Peroxo Dinuclear Copper(II) Complexes in the Millisecond Time Domain (O_2 Rebinding Kinetics). The generated Cu^{I} complexes $[(N5)Cu^{I}_2]^{2+}$ and $[(N3)Cu^{I}_2]^{2+}$ produced by laser excitation of $[(N5)Cu^{II}(O_2^{2-})Cu^{II}]^{2+}$ (**2**) and $[(N3)Cu^{II}(O_2^{2-})Cu^{II}]^{2+}$ (**3**) reacted cleanly with O_2 to regenerate **2** and **3**, respectively. The intermolecular reactions of the Cu^{I} complexes with O_2 were monitored by nanosecond laser flash photolysis at low temperature. This approach is superior to the previously reported "flash-and-trap" experiments that required the inclusion of CO gas and/or other various experimental procedures.[14a,b] Here, we have added in dioxygen at various concentrations to examine $[O_2]$ dependencies, and to also study the variable-temperature kinetics, allowing determination of the second-order rate constants and the activation parameters for the reactions of the Cu^{I} complexes with O_2 (vide infra).

Nanosecond laser excitation of an acetone solution of **2** at −80 °C resulted in formation of $[(N5)Cu^{I}_2]^{2+}$ and O_2 as shown in Figure 7b. The observed bleaching is fully consistent with that expected for the loss of O_2 from the $Cu^{I}_2-O_2$ complex, because subtraction of the absorption spectrum of **2** from that of $[(N5)Cu^{I}_2]^{2+}$ afforded a simulated spectrum (red line in Figure 7b) which agrees well with the observed transient difference spectrum. The absorption change was found to be linear with the laser fluence over the 5−100 mJ cm^{-2} range, indicating that photoinduced release of O_2 is a monophotonic process (Figure S4a). Thus, the laser-induced photoejections of dioxygen from complexes **2** and **3** (see below) are formally very

DOI: 10.1021/jacs.5b10177
J. Am. Chem. Soc. 2015, 137, 15865−15874

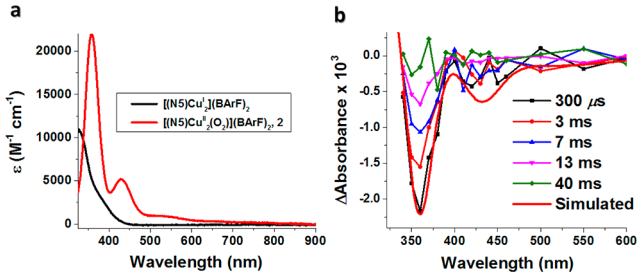

Figure 7. (a) Absorption spectrum of **2** (red line) obtained from oxygenation of $[(N5)Cu^{I}_{2}]^{2+}$ (black line) in acetone at −80 °C. (b) Transient absorption difference spectra collected at the indicated delay times after 532 nm laser excitation (10 mJ/pulse, 8−10 ns fwhm) of **2** in acetone at −80 °C. Overlaid in red on the experimental data is a simulated spectrum (Abs($[(N5)Cu^{I}_{2}(CH_3CN)]^{2+}$), Abs(**2**)), corresponding to the negative of the spectrum of $[(N5)Cu^{II}(O_2{}^{2-})Cu^{II}]^{2+}$ (**2**).

rarely observed (and see further discussion below) one-photon two-electron processes:

$$[(Nn)Cu^{II}(O_2{}^{2-})Cu^{II}]^{2+}(\mathbf{2}\text{ or }\mathbf{3}) + 1\text{ photon} \rightarrow [(Nn)Cu^{I}_{2}]^{2+} + O_{2(g)}$$

Similar transient absorption spectra were observed for nanosecond laser flash photolysis measurements of an acetone solution of the oxygenated complex $[(N3)Cu^{I}_{2}]^{2+}$, i.e., **3**, at −80 °C (Figure 8b) and a quantum yield for photoinduced

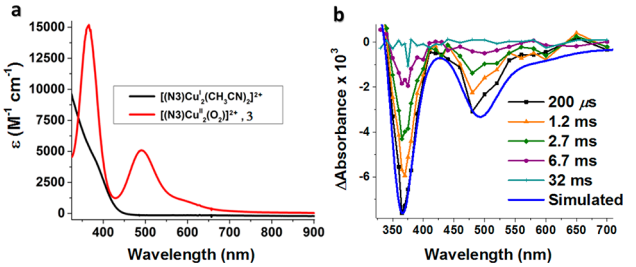

Figure 8. (a) Absorption spectrum of **3** (red line) obtained from oxygenation of $[(N3)Cu^{I}_{2}]^{2+}$ (black line) in acetone at −80 °C. (b) Transient absorption difference spectra collected at the indicated delay times after 532 nm laser excitation (10 mJ/pulse, 8−10 ns fwhm) of **3** in acetone at −80 °C. Overlaid in blue is a simulated spectrum based on subtraction of the red spectrum from the black in (a).

release of O_2 determined at 30 ns after the laser pulse was estimated to be 0.14 ± 0.01 (see the Experimental Section). This value was similar to those previously determined for photoinduced superoxide-to-copper(II) O_2 release from mononuclear copper(II)−superoxide complexes: 0.11 and 0.29.[18a] The rate of recovery of the bleaching observed at 365 nm obeyed first-order kinetics in the presence of excess O_2, and the observed pseudo-first-order rate constant increased linearly with the O_2 concentration (Figure S5).

The second-order rate constants (k_{O_2}) for the reactions of $[(N5)Cu^{I}_{2}]^{2+}$ and $[(N3)Cu^{I}_{2}]^{2+}$ with O_2 were determined at various temperatures as listed in Table 2 and Table S4 in the Supporting Information. The k_{O_2} values determined for $[(N5)Cu^{I}_{2}]^{2+}$ $[(7.0 \pm 1.9) \times 10^3\ M^{-1}\ s^{-1}]$ and $[(N3)Cu^{I}_{2}]^{2+}$ $[(3.8 \pm 1.2) \times 10^3\ M^{-1}\ s^{-1}]$ in acetone at −90 °C are only slightly larger than the corresponding reported values $[(4.1 \pm 0.3) \times 10^3$ and $(1.1 \pm 0.1) \times 10^3\ M^{-1}\ s^{-1}]$ in CH_2Cl_2 at −90 °C, as measured by low-temperature stopped-flow spectroscopy,[8c] possibly due to the difference in solvation.

Table 2. Rate Constants and Activation Parameters for the Reactions of $[(N5)Cu^{I}_{2}]^{2+}$, $[(N3)Cu^{I}_{2}]^{2+}$, Deoxy-Tyr, and Deoxy-Hc with O_2

Cu complex (T)	k_{O_2}, $M^{-1}\ s^{-1}$	$\Delta H^{\ddagger}$ [a]	$\Delta S^{\ddagger}$ [b]
$[(N5)Cu^{I}_{2}]^{2+}$ (−90 °C)	$(7.0 \pm 1.9) \times 10^3$	5 ± 1	−9 ± 5
$[(N3)Cu^{I}_{2}]^{2+}$ (−90 °C)	$(3.8 \pm 1.2) \times 10^3$	8 ± 1	3 ± 6
$[(N5)Cu^{I}_{2}]^{2+}$ (21 °C)	$(3.2 \pm 1.0) \times 10^6$		
$[(N3)Cu^{I}_{2}]^{2+}$ (21 °C)	$(2.8 \pm 1.2) \times 10^7$		
Tyr[c]	1.9×10^7	13 ± 3	
Hc[d]	$(3.1-15.4) \times 10^7$		
Hc[e]	2.3×10^7		

[a]Units for $\Delta H^{\ddagger}$ are kcal mol^{-1}. [b]Units for $\Delta S^{\ddagger}$ are cal K^{-1} mol^{-1}. [c]Reference 20a. [d]Reference 24a. [e]Reference 24b.

Eyring plots of k_{O_2} for $[(N3)Cu^{I}_{2}]^{2+}$ and $[(N5)Cu^{I}_{2}]^{2+}$ are shown in parts a and b, respectively, of Figure 9, and activation

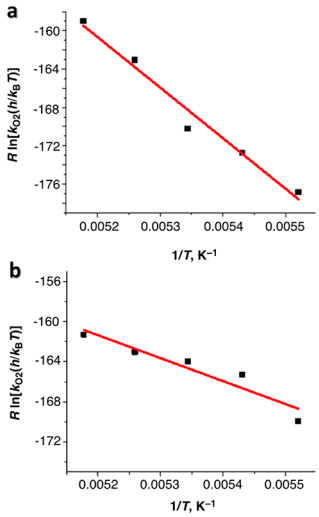

Figure 9. Eyring plots of k_{O_2} for O_2 binding to the dicopper(I) complex $[(N3)Cu^{I}_{2}]^{2+}$, which leads to **3** (a), or $[(N5)Cu^{I}_{2}]^{2+}$, which gives **2** (b), in acetone.

parameters are listed in Table 2. The activation enthalpy found was comparable in the two cases, and a more negative activation entropy for the reaction between $[(N5)Cu^{I}_{2}]^{2+}$ and O_2 suggests, as previously observed,[8c] a greater inner-sphere reorganization energy in this case, probably due to the longer polymethylene chain present in $[(N5)Cu^{I}_{2}]^{2+}$.

The kinetics of O_2 coordination determined here also reveals noticeable similarities to that observed for both the copper-containing proteins hemocyanin (Hc; O_2 carrier in mollusks and arthropods) and tyrosinase (Tyr; ubiquitous *o*-phenol monooxygenase).[1,20,24,25] These proteins possess similar dicopper active sites where each separated copper(I) ion binds three protein-derived histidine imidazole N-donor ligands, and the oxygenated form consists of a $Cu^{II}-(\mu\text{-}\eta^2{:}\eta^2\text{-}O_2{}^{2-})-Cu^{II}$ moiety, the same peroxo binding mode found in $[(N5)Cu^{II}_{2}(O_2)]^{2+}$ (**2**) and $[(N3)Cu^{II}_{2}(O_2)]^{2+}$ (**3**) (Chart 1). Interestingly, the rate constants, when extrapolated at 21 °C, as well as the activation parameters determined here for the formation of **2** and **3** are essentially the same with those previously reported for Tyr[20a] and Hc[20b,24] (Table 2).

DOI: 10.1021/jacs.5b10177
J. Am. Chem. Soc. 2015, 137, 15865−15874

SUMMARY AND CONCLUSION

The present study on the photodynamics of the excited states of $Cu^{II}-O_2$ species opens a new and exciting research area of reactive excited states of metal$-O_2$ intermediates. Here, in summary, we reported on the first unambiguous example of an, overall, one-photon two-electron oxidation, that being the oxidation of peroxide to molecular oxygen occurring when the end-on *trans*-μ-1,2-peroxide dicopper(II) compound $[(tmpa)Cu^{II}(O_2)Cu^{II}(tmpa)]^{2+}$ (**1**) or the side-on μ-η^2:η^2-peroxide complexes $[(N5)Cu^{II}(O_2^{2-})Cu^{II}]^{2+}$ (**2**) and $[(N3)Cu^{II}(O_2^{2-})Cu^{II}]^{2+}$ (**3**) are illuminated with visible light. A stepwise electron transfer mechanism was elucidated employing a novel ultrafast low-temperature transient absorption apparatus, and new intermediates were observed and assigned as a mixed-valent $Cu^{II}(O_2^{\bullet-})Cu^{I}$ species. While complex **1** converted to the "O_2-caged" dicopper(I) complex $[(tmpa)Cu^{I}(O_2)Cu^{I}(tmpa)]^{2+}$ without O_2 release, femtosecond illumination of complexes **2** and **3** under the same conditions showed a remarkably different behavior such that the observed mixed-valent Cu^{II}−superoxide−Cu^{I} intermediates derived from these complexes further decay to two Cu^{I} ions, with complete release of O_2 via electron transfer from the superoxide ligand to the Cu^{II} moiety. Thus, the results imply that, in the O_2-binding process, certainly for oxygenation of $[(N5)Cu^{I}_2]^{2+}$ and $[(N3)Cu^{I}_2]^{2+}$, a transient mixed-valent species ($[(Nn)Cu^{II}(O_2^{\bullet-})Cu^{I}]^{2+}$) forms first (see the equation below); it is however unobservable because the initial reaction of O_2 with one cuprous ion resides in a strongly left-lying equilibrium and the reaction with the second cuprous ion is fast (see also below).[8c] The only manner to observe the $Cu^{II}(O_2^{\bullet-})Cu^{I}$ species is as described here, the use of laser photolysis starting with the peroxodicopper(II) complexes.

$$[(Nn)Cu^{I}_2]^{2+} + O_{2(g)} \leftrightarrow [(Nn)Cu^{II}(O_2^{\bullet-})\cdots Cu^{I}]^{2+} \rightarrow [(Nn)Cu^{II}(O_2^{2-})Cu^{II}]^{2+}$$

The different reaction pathways observed for the end-on (**1** in Scheme 2) and the side-on (**2** in Scheme 4 and complex **3**) peroxo complexes may be thought of and explained in terms of the known much lower ligand$-Cu^{II/I}$ reduction potentials (as determined by prior cyclic voltammetric measurements) on isolated ligand−copper(I) complexes (ligands: tmpa, N3, N5, or PY2). For tmpa$-Cu^{I}$, E° = 0.05 V vs SCE in acetone,[14a,26,28] as compared with that for Cu^{I} with PY2 moieties as found in **2** or **3** (E° = +0.37 V vs SCE in acetone).[8d,27,28] Thus, back electron transfer from the Cu^{I} ion to O_2 is favored in $[(tmpa)Cu^{I}(O_2)Cu^{I}(tmpa)]^{2+}$ (Scheme 2) {and in mixed-valent $[(tmpa)Cu^{II}(O_2^{\bullet-})Cu^{I}(tmpa)]^{2+}$} in comparison to the possible O_2 release and production of 2 equiv of $[(tmpa)Cu^{I}]^{+}$. By contrast, O_2 release from $[(N5)Cu^{I}_2(O_2)]^{2+}$ and then the N5 mixed-valent $[(N5)Cu^{II}(O_2^{\bullet-})Cu^{I}]^{2+}$ species is favored in comparison to the much slower back electron transfer from Cu^{I} to O_2 in these intermediates (Scheme 4).

The disparate $Cu^{II/I}$ reduction potentials in the two classes of compounds result from the presence of an additional N-donor atom bound to each Cu^{I} in the compounds derived from **1** compared to those derived from **2** and **3** (tetradentate tmpa vs tridentate N3 and N5), on one hand, and the different chelate ring sizes in the two cases (five-membered ring for **1** vs six-membered ring for **2** and **3**),[8b] on the other hand, which confer different coordination environments, peroxo binding modes, and electronic properties to the resulting O_2 adducts. These variations translate into dramatic effects in electron transfer thermodynamics and kinetics, including the ability to photo-release molecular oxygen for complexes **2** and **3** but not for **1**.

It is interesting to note that, in an earlier computational study from Metz and Solomon[29] on O_2 binding to deoxy-Hc, the findings were that the process proceeds via a simultaneous double electron transfer between the two cuprous ions and O_2, such that, as dioxygen interacts with the first copper ion, the two copper ions approach each other and then the redox reaction occurs: $Cu^{I}\cdots Cu^{I}$ (~4.3 Å separation) + O_2 → $Cu^{II}(O_2)Cu^{II}$ (~3.6 Å Cu−Cu distance). The intermediacy of a discrete $Cu^{II}-O_2^{\bullet-}-Cu^{I}$ initial adduct was ruled out. Thus, our synthetic analogue compounds (i.e., models) behave differently from the dicopper center found in that very special protein environment. The results observed here may be ascribed to the larger $Cu^{I}\cdots Cu^{I}$ average distances likely found in the "floppy" $[(N5)Cu^{I}_2]^{2+}$ and $[(N3)Cu^{I}_2]^{2+}$ complexes. In the Cu^{I}_2/O_2 reactions, the cuprous ion in a $Cu^{II}(O_2^{\bullet-})Cu^{I}$ species is likely to initially not be close to the superoxide moiety. Supporting this view are findings in the solid state, where Cu···Cu distances in nonbridged dicopper complexes with N3, N4, or N5 ligands can vary from ~6 to 10 Å,[8d,e] and as explained above, the initial unfavorable interaction of O_2 with a single cuprous ion in a PY2 environment precludes the possibility of detecting a mixed-valent $Cu^{II}(O_2^{\bullet-})Cu^{I}$ intermediate species in the "forward" $[(Nn)Cu^{I}_2]^{2+}$ + O_2 direction.

Single-photon absorption reactions that drive two-electron transfer reactions are relatively rare yet important for photocatalytic multielectron transfer reactions. A highly relevant example is water oxidation to molecular oxygen that in addition to proton management requires four redox equivalents: two to form the O−O bond in peroxide and an additional two to yield dioxygen gas.[30] The last two are particularly important as the release of peroxide or superoxide can give rise to unwanted radical chemistry. The peroxide-to-copper charge transfer absorption bands reported herein harvest sunlight across the entire visible region, and their photoreactivity indicates that, with the proper peroxide coordination environment, light excitation does indeed drive the two-electron transfer release of dioxygen. It is interesting to speculate whether such photoreactivity may also be included in the realm of newly discovered copper water oxidation catalysts.[31]

EXPERIMENTAL SECTION

Materials. All materials purchased were of the highest purity available from Sigma-Aldrich Chemical or Tokyo Chemical Industry (TCI) and were used as received, unless specified otherwise. Tetrahydrofuran for the synthesis was distilled under an inert atmosphere from Na/benzophenone and degassed with argon prior to use. Pentane and acetone were freshly distilled from calcium hydride and calcium sulfate, respectively, under an inert atmosphere and degassed prior to use. The tmpa ligand,[7] the N3 and N5 ligands,[8c] and the $[Cu^{I}(CH_3CN)_4](BArF)$ complex[32] (BArF = $B(C_6F_5)_4^-$) were synthesized according to literature procedures. $[(N3)Cu^{I}_2(CH_3CN)](BArF)_2$ and $[(N5)Cu^{I}_2(CH_3CN)](BArF)_2$ were synthesized by adding $[Cu^{I}(CH_3CN)_4](BArF)$ (410 mg, 0.452 mmol) to either N3 (114 mg, 0.230 mmol) or N5 (120 mg, 0.230 mmol) in dry, air-free tetrahydrofuran (THF) (15 mL), and the resulting solution was allowed to stir for 30 min. The isolation of the compounds was afforded by precipitation, under an argon atmosphere, in dry, deoxygenated pentane (60 mL). The yellow powders obtained were reprecipitated from THF/pentane (10 mL/60 mL) three times, in both cases. The identities and purities of the ligands and complexes were verified by elemental analysis and/or ^{1}H NMR spectroscopy (see

DOI: 10.1021/jacs.5b10177
J. Am. Chem. Soc. 2015, 137, 15865−15874

Figures S6−S9 in the Supporting Information). Synthesis and manipulations of copper salts were performed according to standard Schlenk techniques or in an MBraun glovebox (with O_2 and H_2O levels below 1 ppm). UV−vis spectra were recorded with a Cary 50 Bio spectrophotometer equipped with a liquid nitrogen chilled Unisoku USP-203-A cryostat. NMR spectroscopy was performed on Bruker 300 and 400 MHz instruments with spectra calibrated to either internal tetramethylsilane (TMS) standard or to residual protio solvent.

Determination of O_2 Solubility in Acetone. Both the solubility of O_2 in acetone at 25 °C (0.011 34 mol/L) and the solubility at different temperatures were determined using data from temperature-dependent studies previously carried out.[33] The formula used for the temperature dependence of the molar fraction solubility of O_2 in acetone is given by the following equation:

$$\ln \chi = -24.3100 + (649.40/T) + [2.6414(\ln T)] \quad (1)$$

where χ is the molar fraction solubility of O_2 in acetone and T is the absolute temperature.

Gas Mixing. Dioxygen (O_2; Air Gas East, grade 4.4) was dried by passing the gas through a short column of supported P4010 (Aquasorb, Mallinckrodt). Red rubber tubing (Fisher Scientific, inner diameter 1/4 in., thickness 3/16 in.) was used to attach the gas cylinders fitted with appropriate regulators to two MKS Instruments Mass-Flo controllers (MKS type 1179A) regulated by an MKS Instruments multichannel flow ratio/pressure controller (MKS type 647C). The gas mixtures, N_2/O_2, were determined by the set flow rates of the two gases. For example, a 10% O_2 mixture would be made by mixing O_2 at a rate of 10 sccm (standard cubic centimeters per minute) with N_2 at 90 sccm for a total flow of 100 sccm. By varying the ratio of O_2 and N_2 with the gas mixer, the concentrations of the gases were determined by taking the percentage of the gas added and multiplying by the solubility of the corresponding gas in acetone.

Transient Absorption Measurements. The sources for the pump and probe pulses for the femtosecond laser spectroscopy performed here were derived from the fundamental output of Integra-C (780 nm, 2 mJ/pulse, and fwhm = 130 fs) at a repetition rate of 1 kHz. A total of 75% of the fundamental output of the laser was introduced into TOPAS, which has optical frequency mixers resulting in a tunable range from 285 to 1660 nm, while the rest of the output was used for white light generation. Prior to generation of the probe continuum, a variable neutral density filter was inserted into the path to generate a stable continuum, and then the laser pulse was fed to a delay line that provides an experimental time window of 3.2 ns with a maximum step resolution of 7 fs. In our experiments, a wavelength of 490 nm of the TOPAS output, which is the fourth harmonic of signal or idler pulses, was chosen as the pump beam. As this TOPAS output consists of not only the desirable wavelength but also unnecessary wavelengths, the latter were deviated using a wedge prism with a wedge angle of 18°. The desirable beam was irradiated at the sample dell with a spot size of 1 mm diameter, where it was merged with the white probe pulse in a close angle (<10°). The probe beam after passing through the 2 mm sample cell put into a Unisoku CoolSpeK (USP-203-BTT-OF) cryostat was focused on a fiber optic cable that was connected to a charge-coupled device (CCD) spectrograph for recording the time-resolved spectra (450−800 nm). Typically, 2500 excitation pulses were averaged for 3 s to obtain the transient spectrum at a set delay time. Kinetic traces at appropriate wavelengths were assembled from the time-resolved spectral data.

Experimental information for the setup of the Nd:YAG flash photolysis apparatus has been previously reported.[34] The apparatus used for nanosecond laser spectroscopy was equipped with a liquid nitrogen chilled Unisoku USP-203-A cryostat. The samples, $[(N5)Cu^{II}_2(O_2)](BArF)_2$ and $[(N3)Cu^{II}_2(O_2)](BArF)_2$, were irradiated with λ_{ex} = 532 nm pulsed light (10 mJ/pulse), and data were collected at the monitored wavelengths from the averages of 30 laser pulses. Samples (about 70 μM) were prepared under an inert atmosphere (drybox) in 1 cm quartz cuvettes with four polished windows made custom by Quark glass. The cuvettes were equipped with a 14/20 joint and Schlenk stopcock. Gas mixtures were added to the sample solutions by direct bubbling through a 24 in. needle (19 gauge) 10 times for 5 s each with intervals of 10 s between each time. During data collection, the gas flowed through the headspace of the sample solution into the cuvette.

Quantum Yield Determination. The quantum yield for dioxygen release from complex **3** was determined in acetone solvent at −80 °C for the 532 nm excitation wavelength. Samples were prepared by bubbling $O_{2(g)}$ in solutions of $[(N3)Cu^{I}_2(CH_3CN)](BArF)_2$ in dried and distilled acetone at −80 °C. The absorbance of the samples at 532 nm (i.e., 0.14 at 532 nm) was monitored using a Cary 50 Bio spectrophotometer equipped with a liquid nitrogen chilled Unisoku USP-203-A cryostat. $[Ru(bpy)_3]Cl_2$ (bpy = 2,2′-bipyridine) in CH_3CN at room temperature was used as an actinometer, and the solutions were prepared to match the optical density at 532 nm. Data collection for the change in absorbance (ΔA) at the corresponding λ_{max} values (365 nm) where the change in extinction coefficients ($\Delta\Sigma$) is known was performed. The quantum yield for dioxygen release from complex **3** was calculated using the following equation:

$$\Phi = (\Delta A_{365,Cu}/\Delta A_{450,actin})(\Delta\Sigma_{450,actin}/\Delta\Sigma_{365,Cu})(n_{acetone}^2/n_{CH_3CN}^2) \quad (2)$$

where "actin" is $[Ru(bpy)_3]Cl_2$ in CH_3CN at room temperature. The values used were $\Delta\Sigma_{450,actin} = -10\,600\ M^{-1}\ cm^{-1}$[35] and $\Delta\Sigma_{365,Cu} = -7264\ M^{-1}\ cm^{-1}$, with the latter determined in this work. For the refractive index, the value 1.341 63 for CH_3CN (n_{CH_3CN}) at 298.15 K was used,[36] whereas a temperature correction of 0.000 45 per kelvin was added to the refractive index of acetone at 293.15 K (1.359)[37] to obtain the refractive index which was used for acetone at 193.15 K in eq 2: $n_{acetone} = 1.359 + [0.00045(293.15 - 193.15)] = 1.404$.

Eyring Plots. Samples were prepared for the laser experiments by bubbling O_2 gas into acetone solutions of the corresponding Cu^I complex. For example, O_2 was added to an acetone solution of $[(tmpa)Cu^{I}(CH_3CN)](BArF)$ (976 μM) at low temperature to generate **1**. Laser measurements were performed in a temperature range from −94 to −55 °C, and data were fitted with the Eyring equation:

$$\ln(kh/k_BT) = -\Delta H^{\ddagger}/(RT) + \Delta S^{\ddagger}/R \quad (3)$$

where h is the Planck constant, k_B is the Boltzmann constant, and k is the rate constant. Temperature dependence studies were performed in this work using 436, 490 and 532 nm excitation wavelengths.

■ ASSOCIATED CONTENT

Supporting Information

The Supporting Information is available free of charge on the ACS Publications website at DOI: 10.1021/jacs.5b10177.

Tables listing the rate constants for electron transfer and second-order rate constants and figures showing the determination of λ_{max}, laser pulse energy dependence, representative kinetic traces, ^{1}H NMR spectra, and elemental analysis results (PDF)

■ AUTHOR INFORMATION

Corresponding Authors

*karlin@jhu.edu

*fukuzumi@chem.eng.osaka-u.ac.jp

Present Address

⊥G.J.M.: Department of Chemistry, University of North Carolina, Chapel Hill, NC 27599.

Notes

The authors declare no competing financial interest.

DOI: 10.1021/jacs.5b10177
J. Am. Chem. Soc. 2015, 137, 15865−15874

■ ACKNOWLEDGMENTS

S.F. acknowledges research support for the ALCA and SENTAN projects from JST, Japan. K.D.K. acknowledges financial support of this research from the National Institutes of Health, Grant R01 GM28962. G.J.M. is grateful for research support from the National Science Foundation, Grant CHE-1517916.

■ REFERENCES

(1) (a) Solomon, E. I.; Heppner, D. E.; Johnston, E. M.; Ginsbach, J. W.; Cirera, J.; Qayyum, M.; Kieber-Emmons, M. T.; Kjaergaard, C. H.; Hadt, R. G.; Tian, L. *Chem. Rev.* **2014**, *114*, 3659−3853. (b) Solomon, E. I.; Ginsbach, J. W.; Heppner, D. E.; Kieber-Emmons, M. T.; Kjaergaard, C. H.; Smeets, P. J.; Tian, L.; Woertink, J. S. *Faraday Discuss.* **2011**, *148*, 11−39.

(2) (a) Cramer, C. J.; Tolman, W. B. *Acc. Chem. Res.* **2007**, *40*, 601−608. (b) Lewis, E. A.; Tolman, W. B. *Chem. Rev.* **2004**, *104*, 1047−1076. (c) Mirica, L. M.; Ottenwaelder, X.; Stack, T. D. P. *Chem. Rev.* **2004**, *104*, 1013−1045. (d) Kitajima, N.; Moro-oka, Y. *Chem. Rev.* **1994**, *94*, 737−757.

(3) (a) Suzuki, M. *Acc. Chem. Res.* **2007**, *40*, 609−617. (b) Koval, I. A.; Gamez, P.; Belle, C.; Selmeczi, K.; Reedijk, J. *Chem. Soc. Rev.* **2006**, *35*, 814−840.

(4) (a) Fukuzumi, S.; Karlin, K. D. *Coord. Chem. Rev.* **2013**, *257*, 187−195. (b) Fukuzumi, S.; Yamada, Y.; Karlin, K. D. *Electrochim. Acta* **2012**, *82*, 493−511. (c) Fukuzumi, S. *Dalton Trans.* **2015**, *44* (15), 6696−6705.

(5) (a) Itoh, S.; Fukuzumi, S. *Acc. Chem. Res.* **2007**, *40*, 592−600. (b) Kodera, M.; Kano, K. *Bull. Chem. Soc. Jpn.* **2007**, *80*, 662−676. (c) Itoh, S.; Fukuzumi, S. *Bull. Chem. Soc. Jpn.* **2002**, *75*, 2081−2095.

(6) Hatcher, L. Q.; Karlin, K. D. *Adv. Inorg. Chem.* **2006**, *58*, 131−184.

(7) (a) Jacobson, R. R.; Tyeklar, Z.; Farooq, A.; Karlin, K. D.; Liu, S.; Zubieta, J. *J. Am. Chem. Soc.* **1988**, *110*, 3690−3692. (b) Baldwin, M. J.; Ross, P. K.; Pate, J. E.; Tyeklar, Z.; Karlin, K. D.; Solomon, E. I. *J. Am. Chem. Soc.* **1991**, *113*, 8671−8679. Tyeklar, Z.; Jacobson, R. R.; Wei, N.; Murthy, N. N.; Zubieta, J.; Karlin, K. D. *J. Am. Chem. Soc.* **1993**, *115*, 2677−2689.

(8) (a) Karlin, K. D.; Kaderli, S.; Zuberbühler, A. D. *Acc. Chem. Res.* **1997**, *30*, 139. (b) Hatcher, L. Q.; Karlin, K. D. *JBIC, J. Biol. Inorg. Chem.* **2004**, *9*, 669−683. (c) Liang, H.-C.; Karlin, K. D.; Dyson, R.; Kaderli, S.; Jung, B.; Zuberbühler, A. D. *Inorg. Chem.* **2000**, *39*, 5884−5894. (d) Karlin, K. D.; Tyeklár, Z.; Farooq, A.; Haka, M. S.; Ghosh, P.; Cruse, R. W.; Gultneh, Y.; Hayes, J. C.; Toscano, P. J.; Zubieta, J. *Inorg. Chem.* **1992**, *31*, 1436−1451. (e) Thyagarajan, S.; Murthy, N. N.; Narducci Sarjeant, A. A.; Karlin, K. D.; Rokita, S. E. *J. Am. Chem. Soc.* **2006**, *128*, 7003−7008.

(9) (a) Helton, M. E.; Chen, P.; Paul, P. P.; Tyeklar, Z.; Sommer, R. D.; Zakharov, L. N.; Rheingold, A. L.; Solomon, E. I.; Karlin, K. D. *J. Am. Chem. Soc.* **2003**, *125*, 1160−1161. (b) Lee, Y.; Lee, D.-H.; Park, G. Y.; Lucas, H. R.; Narducci Sarjeant, A. A.; Kieber-Emmons, M. T.; Vance, M. A.; Milligan, A. E.; Solomon, E. I.; Karlin, K. D. *Inorg. Chem.* **2010**, *49*, 8873−8885.

(10) (a) Dalle, K. E.; Gruene, T.; Dechert, S.; Demeshko, S.; Meyer, F. *J. Am. Chem. Soc.* **2014**, *136*, 7428−7434. (b) Porras Gutiérrez, A. G.; Zeitouny, J.; Gomila, A.; Douziech, B.; Cosquer, N.; Conan, F.; Reinaud, O.; Hapiot, P.; Le Mest, Y.; Lagrost, C.; Le Poul, N. *Dalton Trans.* **2014**, *43*, 6436−6445.

(11) (a) Park, G. Y.; Qayyum, M. F.; Woertink, J.; Hodgson, K. O.; Hedman, B.; Narducci Sarjeant, A. A.; Solomon, E. I.; Karlin, K. D. *J. Am. Chem. Soc.* **2012**, *134*, 8513−8524. (b) Shearer, J.; Zhang, C. X.; Zakharov, L. N.; Rheingold, A. L.; Karlin, K. D. *J. Am. Chem. Soc.* **2005**, *127*, 5469−5483.

(12) (a) Rolff, M.; Schottenheim, J.; Decker, H.; Tuczek, F. *Chem. Soc. Rev.* **2011**, *40*, 4077−4098. (b) De, A.; Mandal, S.; Mukherjee, R. *J. Inorg. Biochem.* **2008**, *102*, 1170−1189. (c) Rolff, M.; Tuczek, F. *Angew. Chem., Int. Ed.* **2008**, *47*, 2344−2347. (d) Rolle, C., III; Saracini, C.; Karlin, K. D. *Encyclopedia of Inorganic and Bioinorganic Chemistry*; Johns Wiley & Sons, Ltd.: Chichester, U.K., 2014. http://dx.doi.org/10.1002/9781119951438.eibc0049.pub2.

(13) (a) Himes, R. A.; Barnese, K.; Karlin, K. D. *Angew. Chem., Int. Ed.* **2010**, *49*, 6714−6716. (b) Balasubramanian, R.; Smith, S. M.; Rawat, S.; Yatsunyk, L. A.; Stemmler, T. L.; Rosenzweig, A. C. *Nature* **2010**, *465*, 115−119. (c) Himes, R. A.; Karlin, K. D. *Proc. Natl. Acad. Sci. U. S. A.* **2009**, *106*, 18877−18878. (d) Chan, S. I.; Yu, S. S.-F. *Acc. Chem. Res.* **2008**, *41*, 969−979.

(14) (a) Lucas, H. R.; Meyer, G. J.; Karlin, K. D. *J. Am. Chem. Soc.* **2010**, *132*, 12927−12940. (b) Fry, H. C.; Scaltrito, D. V.; Karlin, K. D.; Meyer, G. J. *J. Am. Chem. Soc.* **2003**, *125*, 11866−11871. (c) Lucas, H. R.; Li, L.; Narducci Sarjeant, A. A.; Vance, M. A.; Solomon, E. I.; Karlin, K. D. *J. Am. Chem. Soc.* **2009**, *131*, 3230−3245. (d) Wagnerova, D. M.; Lang, K. *Coord. Chem. Rev.* **2011**, *255*, 2904−2911. (e) Vogler, A.; Kunkely, H. *Coord. Chem. Rev.* **2006**, *250*, 1622−1626. (f) Fry, H. C.; Hoertz, P. G.; Wasser, I. M.; Karlin, K. D.; Meyer, G. J. *J. Am. Chem. Soc.* **2004**, *126*, 16712−16713. (g) Ye, X.; Demidov, A.; Champion, P. M. *J. Am. Chem. Soc.* **2002**, *124*, 5914−5924.

(15) (a) Garcia-Bosch, I.; Company, A.; Frisch, J. R.; Torrent-Sucarrat, M.; Cardellach, M.; Gamba, I.; Güell, M.; Casella, L.; Que, L., Jr.; Ribas, X.; Luis, J. M.; Costas, M. *Angew. Chem., Int. Ed.* **2010**, *49*, 2406−2409. (b) Mandal, S.; Mukherjee, J.; Lloret, F.; Mukherjee, R. *Inorg. Chem.* **2012**, *51*, 13148−13161. (c) Garcia-Bosch, I.; Ribas, X.; Costas, M. *Chem. - Eur. J.* **2012**, *18*, 2113−2122.

(16) (a) Rolff, M.; Hamann, J. N.; Tuczek, F. *Angew. Chem., Int. Ed.* **2011**, *50*, 6924−6927. (b) Rolff, M.; Schottenheim, J.; Peters, G.; Tuczek, F. *Angew. Chem., Int. Ed.* **2010**, *49*, 6438−6442. (c) Sander, O.; Henss, A.; Näther, C.; Würtele, C.; Holthausen, M. C.; Schindler, S.; Tuczek, F. *Chem. - Eur. J.* **2008**, *14*, 9714−9729.

(17) (a) Matsumoto, T.; Ohkubo, K.; Honda, K.; Yazawa, A.; Furutachi, H.; Fujinami, S.; Fukuzumi, S.; Suzuki, M. *J. Am. Chem. Soc.* **2009**, *131*, 9258−9267. (b) Company, A.; Palavicini, S.; Garcia-Bosch, I.; Mas-Balleste, R.; Que, L., Jr.; Rybak-Akimova, E. V.; Casella, L.; Ribas, X.; Costas, M. *Chem. - Eur. J.* **2008**, *14*, 3535−3538. (c) Osako, T.; Ohkubo, K.; Taki, M.; Tachi, Y.; Fukuzumi, S.; Itoh, S. *J. Am. Chem. Soc.* **2003**, *125*, 11027−11033. (d) Henson, M. J.; Vance, M. A.; Zhang, C. X.; Liang, H.-C.; Karlin, K. D.; Solomon, E. I. *J. Am. Chem. Soc.* **2003**, *125*, 5186−5192. (e) Itoh, S.; Kumei, H.; Taki, M.; Nagatomo, S.; Kitagawa, T.; Fukuzumi, S. *J. Am. Chem. Soc.* **2001**, *123*, 6708−6709.

(18) (a) Saracini, C.; Liakos, D. G.; Zapata Rivera, J. E. Z.; Neese, F.; Meyer, G. J.; Karlin, K. D. *J. Am. Chem. Soc.* **2014**, *136*, 1260−1263. (b) Woertink, J. S.; Tian, L.; Maiti, D.; Lucas, H. R.; Himes, R. A.; Karlin, K. D.; Neese, F.; Wurtele, C.; Holthausen, M. C.; Bill, E.; Sundermeyer, J.; Schindler, S.; Solomon, E. I. *Inorg. Chem.* **2010**, *49*, 9450−9459.

(19) Peterson, R. L.; Himes, R. A.; Kotani, H.; Suenobu, T.; Tian, L.; Siegler, M. A.; Solomon, E. I.; Fukuzumi, S.; Karlin, K. D. *J. Am. Chem. Soc.* **2011**, *133*, 1702−1705.

(20) (a) Hirota, S.; Kawahara, T.; Lonardi, E.; de Waal, E.; Funasaki, N.; Canters, G. W. *J. Am. Chem. Soc.* **2005**, *127*, 17966−17967. (b) Hirota, S.; Kawahara, T.; Beltramini, M.; Di Muro, P.; Magliozzo, R. S.; Peisach, J.; Powers, L. S.; Tanaka, N.; Nagao, S.; Bubacco, L. *J. Biol. Chem.* **2008**, *283*, 31941−31948.

(21) (a) Kunishita, A.; Kubo, M.; Sugimoto, H.; Ogura, T.; Sato, K.; Takui, T.; Itoh, S. *J. Am. Chem. Soc.* **2009**, *131*, 2788−2789. (b) Kunishita, A.; Ertem, M. Z.; Okubo, Y.; Tano, T.; Sugimoto, H.; Ohkubo, K.; Fujieda, N.; Fukuzumi, S.; Cramer, C. J.; Itoh, S. *Inorg. Chem.* **2012**, *51*, 9465−9480. (c) Tano, T.; Okubo, Y.; Kunishita, A.; Kubo, M.; Sugimoto, H.; Fujieda, N.; Ogura, T.; Itoh, S. *Inorg. Chem.* **2013**, *52*, 10431−10437. (d) Donoghue, P. J.; Gupta, A. K.; Boyce, D. W.; Cramer, C. J.; Tolman, W. B. *J. Am. Chem. Soc.* **2010**, *132*, 15869−15871.

(22) Peterson, R. L.; Ginsbach, J. W.; Cowley, R. E.; Qayyum, M. F.; Himes, R. A.; Siegler, M. A.; Moore, C. D.; Hedman, B.; Hodgson, K. O.; Fukuzumi, S.; Solomon, E. I.; Karlin, K. D. *J. Am. Chem. Soc.* **2013**, *135*, 16454−16467.

(23) Radiance-dependent and kinetic data for the decrease of the broad absorption due to $Cu^{II}O_2^{\bullet-}$ were collected at 750 nm instead of

DOI: 10.1021/jacs.5b10177
J. Am. Chem. Soc. 2015, 137, 15865−15874

λ_{max} = 730 nm to minimize the contribution of the overlapping spectral bleach due to the Cu^{I} moiety.
(24) (a) Andrew, C. R.; McKillop, K. P.; Sykes, A. G. *Biochim. Biophys. Acta, Protein Struct. Mol. Enzymol.* **1993**, *1162*, 105−114. (b) Rodríguez-López, J. N.; Fenoll, L. G.; García-Ruiz, P. A.; Varón, R.; Tudela, J.; Thorneley, R. N. F.; García-Cánovas, F. *Biochemistry* **2000**, *39*, 10497−10506.
(25) (a) Magnus, K. A.; Hazes, B.; Ton-That, H.; Bonaventura, C.; Bonaventura, J.; Hol, W. G. *Proteins: Struct., Funct., Genet.* **1994**, *19*, 302−309. (b) Solomon, E. I.; Sundaram, U. M.; Machonkin, T. E. *Chem. Rev.* **1996**, *96*, 2563−2605.
(26) (a) Fukuzumi, S.; Kotani, H.; Lucas, H. R.; Doi, K.; Suenobu, T.; Peterson, R. L.; Karlin, K. D. *J. Am. Chem. Soc.* **2010**, *132*, 6874−6875. (b) Kakuda, S.; Peterson, R. L.; Ohkubo, K.; Karlin, K. D.; Fukuzumi, S. *J. Am. Chem. Soc.* **2013**, *135*, 6513−6522.
(27) (a) Pidcock, E.; Obias, H. V.; Abe, M.; Liang, H.-C.; Karlin, K. D.; Solomon, E. I. *J. Am. Chem. Soc.* **1999**, *121*, 1299−1308. (b) Tahsini, L.; Kotani, H.; Lee, Y.-M.; Cho, J.; Nam, W.; Karlin, K. D.; Fukuzumi, S. *Chem. - Eur. J.* **2012**, *18*, 1084−1093.
(28) (a) Fukuzumi, S.; Tahsini, L.; Lee, Y.-M.; Ohkubo, K.; Nam, W.; Karlin, K. D. *J. Am. Chem. Soc.* **2012**, *134*, 7025−7035. (b) Das, D.; Lee, Y.-M.; Ohkubo, K.; Nam, W.; Karlin, K. D.; Fukuzumi, S. *J. Am. Chem. Soc.* **2013**, *135*, 2825−2834. (c) Das, D.; Lee, Y.-M.; Ohkubo, K.; Nam, W.; Karlin, K. D.; Fukuzumi, S. *J. Am. Chem. Soc.* **2013**, *135*, 4018−4026.
(29) Metz, M.; Solomon, E. I. *J. Am. Chem. Soc.* **2001**, *123*, 4938−4950.
(30) Bard, A. J.; Fox, M. A. *Acc. Chem. Res.* **1995**, *28*, 141−145.
(31) (a) Barnett, S. M.; Goldberg, K. I.; Mayer, J. M. *Nat. Chem.* **2012**, *4*, 498−502. (b) Zhang, M. T.; Chen, Z.; Kang, P.; Meyer, T. J. *J. Am. Chem. Soc.* **2013**, *135*, 2048−2051. (c) Chen, Z.; Meyer, T. J. *Angew. Chem., Int. Ed.* **2013**, *52*, 700−703.
(32) Liang, H. C.; Kim, E.; Incarvito, C. D.; Rheingold, A. L.; Karlin, K. D. *Inorg. Chem.* **2002**, *41*, 2209−2212.
(33) (a) Fogg, P. G. T.; Gerrard, W. *Solubility of Gases in Liquids: A Critical Evaluation of Gas/Liquid Systems in Theory and Practice*; Wiley: Chichester, U.K., 1991. (b) Fischer, K.; Wilken, M. *J. Chem. Thermodyn.* **2001**, *33*, 1285−1308. (c) Battino, R. *IUPAC Solubility Data Series: Oxygen and Ozone*; Pergamon: Oxford, U.K., New York, 1981.
(34) Argazzi, R.; Bignozzi, C. A.; Heimer, T. A.; Castellano, F. N.; Meyer, G. J. *Inorg. Chem.* **1994**, *33*, 5741−5749.
(35) Yoshimura, A.; Hoffman, M. Z.; Sun, H. *J. Photochem. Photobiol., A* **1993**, *70*, 29−33.
(36) Iloukhani, H.; Almasi, M. *Thermochim. Acta* **2009**, *495*, 139−148.
(37) Kurtz, S. S., Jr.; Wikingsson, A. E.; Camin, D. L.; Thompson, A. R. *J. Chem. Eng. Data* **1965**, *10*, 330−334.

DOI: 10.1021/jacs.5b10177
J. Am. Chem. Soc. 2015, 137, 15865−15874